THE JOURNAL OF PHYSICAL CHEMISTRY A

Article

pubs.acs.org/JPCA

Further Insight into the Nature of Ball-Lightning-Like Atmospheric Pressure Plasmoids

David M. Friday, Peter B. Broughton, Tanner A. Lee, Garrett A. Schutz, Jeremiah N. Betz, and C. Michael Lindsay*,†

Department of Chemistry, United States Air Force Academy, USAF Academy, Colorado 80840, United States

ABSTRACT: Known since antiquity, ball lightning is a natural, long-lived plasma-like phenomenon associated with thunderstorms and is not well understood due to its rarity and unpredictability. A recently discovered laboratory phenomenon with striking similarity to ball lightning is observed when a high-power spark is discharged from a cathode protruding from a grounded electrolyte solution. Whereas several investigations of these long-lived plasmas have been reported over the past decade, the underlying chemical and physical processes are still unknown. The present work attempts to gain further insight into this phenomenon by examining the effect of electrolyte pH on the plasmoid and observing the chemical and physical structure of the plasmoid using high-speed schlieren videography and FTIR absorption spectroscopy. The results indicate that the lifetime and size of the plasmoid slightly increase as the pH of isoohmic electrolyte solutions deviate from neutrality. The observed absorption spectra of the plasmoids exhibit absorption cross sections in the 620−700, 1500−1560, 2280−2390, and 3650−4000 cm^{-1} ranges, the last attributed to the presence of water clusters. Finally, schlieren images revealed a single, sharp density gradient at the boundary layer of the top and sides of the expanding ball-shaped plasmoid, and turbulent mixing below the ball.

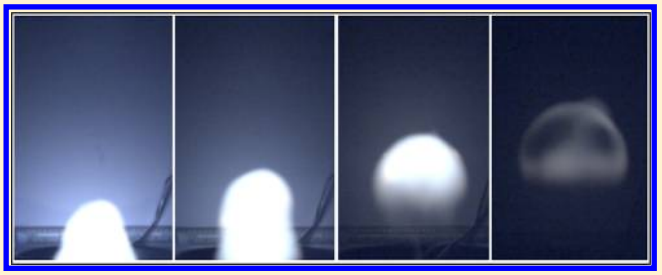

INTRODUCTION

Oka and many others often remind us that nearly the entire Universe is plasma and that Langevin dynamics play a critical role in the chemical equilibrium of such systems.[1−4] From the diffuse interstellar clouds with ion densities $\sim 10^{-2}$ m^{-3} to stellar cores with ion densities as high as 10^{30} m^{-3}, nature exhibits impressive diversity. With all that is known about the ionized environments at the farthest reaches of the Universe, some of which is presented in this Special Issue, it is remarkable that one of the least understood plasmas is found right here on earth and has been known for millennia: ball lightning. Also known as fireballs or *Kugelblitz*, this naturally occurring phenomenon has been the subject of scientific inquiry, mythology, and lore since antiquity. Whereas there are numerous modern theories as to its origins[5−12] the fundamental nature of ball lightning remains an enigma due to its rarity, unpredictability, and spurious behavior. Indeed, it is estimated that the phenomenon occurs with only 1 in 10^6 lightning strikes, and the odds of a person observing it in their lifetime is 1 in 1000.[5,13]

From the thousands of reputable (and otherwise) accounts dating back to Aristotle, it is generally accepted that ball lightning is associated with thunderstorms, yet remarkably there have been few reports of direct observations of a lightning bolt followed by a ball-lightning event.[14] Several reviews over the last century have attempted to summarize the object's properties from eye-witness reports.[6,13−15] Ball lightning is generally described as a glowing body, roughly spherical in shape, ranging in size from a few centimeters to tens of centimeters and generally maintaining a constant luminosity throughout its life. The objects are frequently reported as moving (floating) distances of meters during their lifetime, an indication that the object is not continuously supported by the initial discharge event. Perhaps the most extraordinary property is its longevity. Observers of the phenomenon commonly report lifetimes of the luminous balls of 1−10 s, a remarkable feat if indeed these are unsupported plasma at atmospheric pressure and low temperature.[14,15] Given the wide range of physical conditions under which events have been reported in nature, however, it is quite likely that ball lightning is not a single phenomenon but a collection of physical phenomena that gives rise to similar observables.[13]

The first reproducible experimental production of ball-lightning-like phenomena is attributed to Nicola Tesla during his infamous year at the Colorado Springs laboratory in 1899−1900.[16] In January 1900, Tesla noted that "the phenomenon of the 'fireball' is produced by the sudden heating, to high incandescence, of a mass of air or other gas as the case may be, by the passage of a powerful discharge." Over the last century, there have been numerous attempts to produce atmospheric

Special Issue: Oka Festschrift: Celebrating 45 Years of Astrochemistry

Received: January 1, 2013
Revised: June 13, 2013

   dx.doi.org/10.1021/jp400001y | J. Phys. Chem. A XXXX, XXX, XXX−XXX

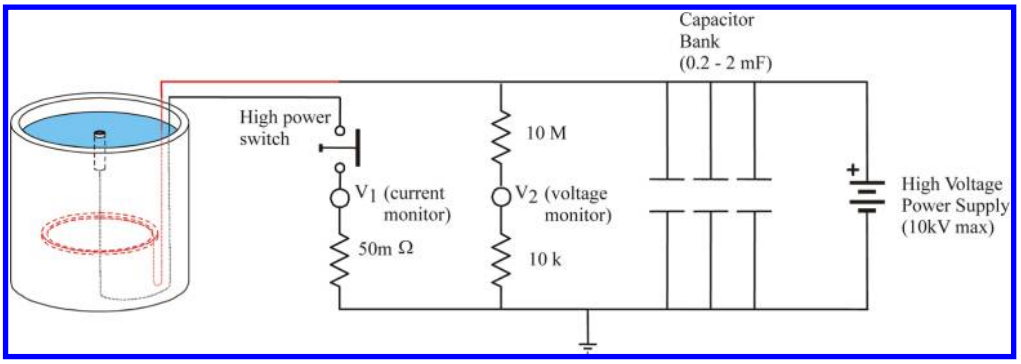

Figure 1. Schematic diagram of the plasmoid generator.

pressure plasmas in general or reproduce Tesla's fireballs with limited success,[15,17,18] the most noteworthy in the works of Kapitza[19,20] and Golka.[21] More recently 'Franklinian' attempts to create ball lightning by harnessing natural bolts of lightning have also proven to be unsuccessful.[22] Over the last 10 years, however, two types of laboratory experiments that resemble ball lightning have shown considerable promise. The first involves the electrically induced combustion of silicon in air[23−25] after low voltage/high current discharges are passed through silicon wires, wafers, or in carbon/silica soil. The second type involves a glow discharge produced above aqueous electrolyte solutions. This paper investigates the latter type, which we herein call atmospheric pressure 'plasmoids.'

In an effort to produce conditions similar to those observed in natural ball lightning, Egorov and Stepanov in Russia studied the behavior of discharges in warm air saturated with water vapor.[28] In 2002 they discovered that when a high current spark is emitted from a wet cathode slightly protruding from a grounded aqueous electrolyte solution a luminous plasmoid emerges from the solution and remains glowing for as long as 1 s. Further investigations by the same group[27,28] estimated the temperature of the plasmoid to be ∼300 K from the rate of increase in the buoyant mass, determined that the emitted color is controlled by the cathode material and the salts used in the electrolyte, and observed that the plasmoid is surrounded by a negatively charged skin. Several years after the initial discovery, Tanabe and collaborators in Japan published a series of papers reporting the time dependence of the visible emission spectrum,[29] dependence of the emission lifetime on some of the electrical properties of the discharge,[30] and identification of the three sequential processes involved in the formation of the plasmoid.[31] Kuleshov and coworkers in Ukraine studied a similar setup and proposed that a critical step in the plasmoid formation is the generation of an acoustically driven plasma column in the aqueous solution, produced by the discharge's shock wave.[32,33] This group also observed that the lifetime of the plasmoid is very sensitive to the temperature of the electrolyte, preferring lower temperatures.[34] Similar experiments were reproduced with additional diagnostics by a group in Germany, including time-resolved high-resolution emission spectroscopy (300−800 nm), laser deflection measurements, and misc probes of the plasma (Langmuir, thermocouple, etc.).[35−38] The main conclusions of their work are that the plasmoid consists of a hot core surrounded by cool shell, possessing a translational temperature ∼600−1300 K, an electron temperature (from various atomic emissions) of 2000−5000 K, and a rotational temperature (OH $A^2\Sigma^+$-$X^2\Pi$) of ∼15 000 K. They also estimated from spectral Stark broadening that the ion density is as high as 10^{22} m^{-3} (∼ 0.1%) in the first 75 ms of the discharge. Experiments have been performed more recently by two different U.S. groups with complementary results[39] and measures of the shock front speeds in the surface discharge.[40]

Whereas these experiments have shed considerable light on many aspects of this plasmoid, there remains much to be understood, in particular, the optimal conditions to produce its features, details of the long-lived emission of light, and the internal chemical and physical structure of the plasmoid. This investigation aims to compliment the previous works, providing additional insight into this phenomenon. First, after characterizing the discharge conditions that influence the lifetime of the plasmoid as has been done in the past, we examine the effect that electrolyte pH has on the vitality of the plasmoid. Second, we image the plasmoid using high-speed schlieren techniques to directly examine its time-dependent internal density structure. Finally, an FTIR spectrometer is used to measure the low-resolution infrared absorption spectrum of the plasmoid.

■ EXPERIMENTAL SECTION

The plasma generator's design was similar to the ones described in previous papers[26,29,36] and was composed of a ring anode placed in an electrolyte solution and a wet cathode protruding from the surface. The copper ring anode with a radius of 9.2 cm, an annular width of 1 cm, and a thickness of 2 mm (10" Conflat Copper Gasket) was submerged 11 cm below the surface of an electrolyte solution. The cathode was produced by sliding a 6.0 mm diameter graphite rod into an alumina tube (wall thickness = 1.5 mm) such that the ceramic casing extended 1 mm above the top surface of the graphite. The bottom of the graphite rod was in contact with high-voltage wire using a copper barrel connector and wrapped with electrical shrink tubing for insulating the conductors from the electrolyte. This cathode was oriented vertically, positioned at the center of the ring and protruded 2 mm above the surface of the electrolyte solution. Before each trial, 50 μL of the electrolytic solution was pipetted on top of the graphite electrode.

The electrolyte solutions were made by adding salts to deionized water. For all trials (except when studying pH) $CuSO_4$ was used to vary the resistivity of the solution from 1.3 to 11 kΩ·cm. When varying the pH of the solution, combinations of HCl, NaOH, and NaCl were used, all the while maintaining a constant resistivity of 5.0 kΩ·cm between trials. Resistance was measured within ±3% error using a

dx.doi.org/10.1021/jp400001y | J. Phys. Chem. A XXXX, XXX, XXX−XXX

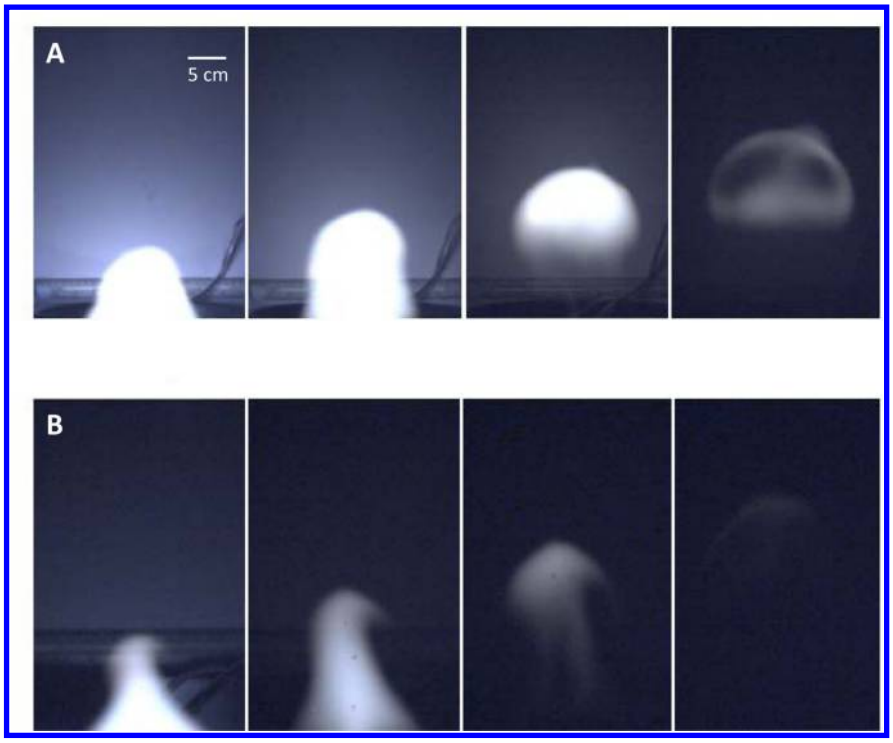

Figure 2. Example visible video images of the plasmoid emerging from a 3kΩ·cm $CuSO_4$ solution by discharging an 860 μF (A) or 270 μF (B) capacitor bank that had been charged to 4800 V. The larger capacitance (energy) discharges produce better-formed, larger, and longer-lived plasmoids.

benchtop analyzer, and pH was measured within ±5% error using a Beckman series 11 pH meter.

Figure 1 shows the schematic diagram of the electrical circuit. A Glassman EK Series high-voltage power supply charged large capacitors to 2−7 kV in current-limiting mode. Three Maxwell oil-filled electrolytic capacitors were used (one 270 μF and two 860 μF), which could be connected in parallel, giving a total capacitance range of 270−1720 μF. The discharge was triggered by Ross Engineering high-voltage E-Series relays. The voltage and current of the circuit were measured through a high-impedance parallel voltage divider and high-power, low-impedance series resistor, respectively, at 1 kHz sample rates using a NI USB-6009 digitizer. Under the conditions investigated in these experiments, peak discharge currents varied from 2 to 126 A.

The plasmoid's visible and infrared emission was recorded by a Pixelink PL-B742U video camera, two silicon photodiodes, and a PbSe photodiode. The RGB video camera sampled at 85 fps through a 16 mm, f/1.4, 2/4" Computar 08J lens. The camera was positioned 150 cm away and 25 cm above the top of the cathode to reveal a 50 cm (horizontal) × 35 cm (vertical) imaged window at the depth of the plasmoid. The silicon diodes (Thorlab model DET 36A, bandwidth 350−1100 nm) were located horizontally 50 cm away from the cathode and positioned at 5 and 35 cm above top of the cathode and sampled at 1 kHz. The infrared photodiode (Thorlabs PDA 20H, bandwidth 1.5−4.8 μm) was located halfway between the two silicon photodiodes and also sampled at 1 kHz. No focusing optics were placed in front of the photodiodes, and their angular field of view was ∼150°.

The lifetime of each plasmoid was determined by counting the number of frames where the plasmoid's emission was observable in the video, starting with the first frame where the cathode discharge is visibly observed. These measurements were in quantitative agreement with the silicon photodiode data. The latter were not used explicitly for lifetime measurements, however, because in some instances, the cathode glowed for long periods of time, producing background light in the photodiode signals, and thus made it difficult to judge the end of the life of the plasmoid from the photodiode signals alone. This other source of light is easily distinguished from the plasmoid in the video images and thus provided a more reliable means of quantifying plasmoid's lifetime. The infrared photodiode signal exhibited nearly identical rise times to the silicon diodes but yielded significantly longer decays. We attributed this observation to the fact that the field of view includes the top of the cathode and surface of the electrolyte, which remain warm for a longer period of time after the event, thereby emitting detectable infrared black/greybody radiation. Indeed, this hypothesis is consistent with unpublished FLIR camera measurements taken of similar plasmoids by Wurden.[41]

The infrared absorption spectrum of the plasmoid was obtained using a Perkin-Elmer Spectrum One FTIR. In the sample compartment of the instrument, the infrared beam was coupled into PIR or CIR mid-infrared fiber optic cables (2300−550 or 5000−1500 cm^{-1}, respectively) and coupled out of the fiber with f = 14 mm, 2.5 cm diameter ZnSe lenses. The approximately collimated infrared beam was then passed through open air with a path length of 32 cm, located 15 cm above the top of the cathode. After passing through the plasma region, the light was coupled into a second fiber that returned the beam back to the sample compartment and into the detector of the FTIR. It is important to note that the infrared light from the instrument had already passed through the interferometer before probing the plasmoid region; therefore, infrared radiation emitted by the plasmoid that happens to be collected by the fibers will not be modulated by the scanning interferometer and thus will be completely rejected from the

dx.doi.org/10.1021/jp400001y | J. Phys. Chem. A XXXX, XXX, XXX−XXX

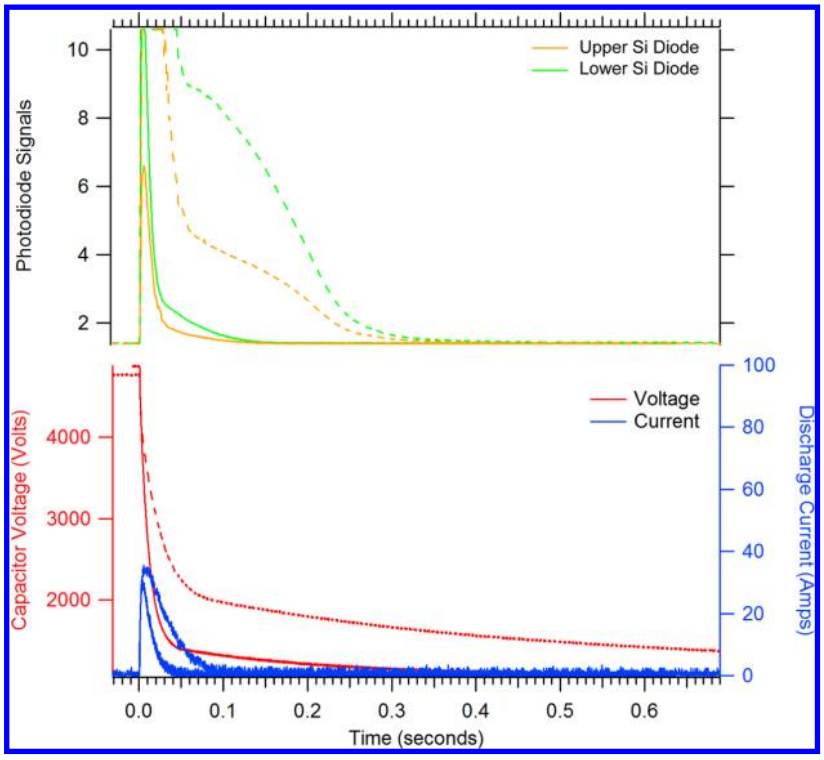

Figure 3. Example discharges' voltage, current, and silicon photodiode signals for plasmoids emerging from a 3kΩ·cm $CuSO_4$ solution, the same events imaged in Figure 1. The dashed lines and solid lines correspond to 860 and 270 μF, respectively. The silicon diodes were located horizontally 50 cm away from the cathode and positioned at 5 (lower, green) and 35 cm (upper, orange) above top of the cathode. Time = 0 is defined as the instant the high-power switch is actuated.

spectrum. Measurements of the plasma event were the average of three scans, with a mirror speed of 1 cm/s and spectral resolution of 4 cm^{-1}. Each transmission spectrum was subtracted from the atmosphere background measurement under the same parameters, except with 64 averaged scans. Plasmoids used in the infrared measurements were produced using 7−9 kΩ·cm $CuSO_4$ solutions, 6 kV, and 860 μF.

High-speed images of the density profiles of the plasmoid were obtained at a different facility using schlieren videography.[42] Light from a Luxeon high-power white LED was collimated with a 30.5 cm diameter spherical mirror and passed ∼3.5 cm above the top of the cathode. After passing through the plasmoid region, the light was refocused with a second, identical mirror, aligned in the standard schlieren z-configuration. A vertically oriented knife edge was placed at the focal point of the second mirror, the position of which was adjusted to produce a schlieren image with maximum contrast. Light beyond the second focal point was imaged into a Phantom V7.0 high-speed camera, which produced high-spatial resolution digital images at a 50 fps rate with a 40 μs exposure time. The time zero of this data set was extrapolated from the first image of the plasmoid using its vertical velocity. The error associated with this method is estimated to be ±1 frame or ±0.02 s. The plasmoids observed in the schlieren photography were produced using a 7.7 kΩ·cm $CuSO_4$ solution, 5 kV, and 860 μF.

RESULTS AND DISCUSSION

Optimizing Discharge and Electrolyte Conditions. The first experiments performed in this work focused on characterizing how the discharge's peak current (I_{max}), capacitance (C), initial capacitor potential (V_0), stored energy in the capacitor bank (E_C), and electrolyte resistivity (R_{elec}) affect the lifetime and diameter of the plasmoid. Figure 2 shows video images of two plasmoids emerging from a 3 kΩ·cm $CuSO_4$ solution at corresponding times. These examples illustrate the effect that total discharge energy has on the plasmoid: the upper frames (A) correspond to an 860 μF capacitor, and the lower frames (B) correspond to a 270 μF capacitor that had each been charged to 4800 V. The total energy stored in the capacitor bank is $E_C = 1/2CV_0^2$, and its total charge is $Q = CV_0$, and thus the upper frames were produced from a discharge with 3.2 times the total charge and energy. It is immediately clear from these images that there is an increase in the plasmoid's lifetime and size with increased capacitance. Both plasmoids are visually identical to those reported by other groups and appear to be generated by the same three-stage plasma process.[27,31,36,39] As others have stated previously, in this case (and in all cases studied in this work) the discharges with larger capacitances produce better formed, larger, and longer-lived plasmoids.[30]

Figure 3 shows the time dependence of the discharge voltage and current for the two trials shown in Figure 2 as well as the silicon photodiodes' signals monitoring the total visible emission of the cathode and above it. In these graphs time = 0 is defined as the instant the high-power switch is actuated. The current and voltage traces show that the discharge from the cathode to the surface of the electrolyte is completed in 50−75 ms and produces an intense light pulse, as detected by the photodiodes with an intensity that follows discharge current. The plasmoid is also observed in the photodiode traces as a second less-intense emission peak that in these particular cases persists for approximately four times longer than the discharge. The integrated intensity of the plasmoid portion of the emission detected by the photodiodes is 15 times higher in the 860 μF event than the 270 μF event, indicating that the

dx.doi.org/10.1021/jp400001y | J. Phys. Chem. A XXXX, XXX, XXX−XXX

luminosity of the plasmoid is not simply governed by its total energy or charge, which is only ~3 times higher.

It is important to point out that as the storage capacitance is increased, two discharge variables are changed: the total charge available to feed the discharge is increased and the duration of the discharge is lengthened. These two effects are coupled by the resistivity of the aqueous solution and can be separated by varying the electrolyte concentration. Figure 4 presents the

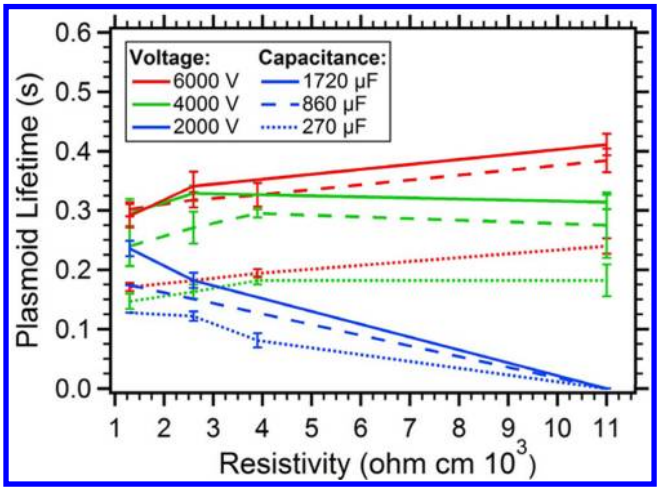

Figure 4. Lifetime of the plasmoid as a function of electrolyte resistivity for different values of voltage (different colors) and capacitance (dots/dashes/lines). The reported error bars represent one standard deviation from replicate measurements.

results of such measurements, examining the plasmoid lifetime as a function R_{elec} for different values of V_0 (different colors) and C (dots/dashes/lines). Examining each trace as the resistivity is increased, we notice that there appears to be a maximum lifetime that varies with voltage; as the resistivity increases, the optimal voltage increases. Indeed, for the highest voltages examined here, the optimum resistivity may not have been reached but potentially lies at even higher resistivity. By comparing traces with different capacitances but fixed voltage, we notice that the peak lifetime appears to shift to higher resistivity as the capacitance decreases, as illustrated by the 4000 V trials (green traces). The fact that both higher voltage discharges and lower capacitance discharges favor higher resistivity suggests that there may be an optimal time frame in which to discharge the energy. Indeed, when we examine the duration of the current pulse for the maximum lifetime conditions in the 4000 V discharges (green traces), they lie within a range 40−65 ms. Figure 5 plots the plasmoid lifetime for all of the electrolyte conditions, normalized to the longest lived trial for a given C and V_0. While there is much uncertainty in these values due in part to the low number of resistivities tested, these preliminary data suggest a steep reduction in the lifetime for very short (<20 ms) duration discharges and a more gentle roll-off for longer discharges durations above 70−100 ms. The former implies that the initial formation of the plasmoid takes tens of milliseconds to evolve, and releasing the charge too quickly does not allow time for the cloud to increase charge density. The latter is consistent with the video images, which show the plasmoid emission visually separated from the cathode 150−200 ms after discharge initiation, meaning that current flow after this window of opportunity cannot provide energy to the ball. This phenomenon needs to be examined

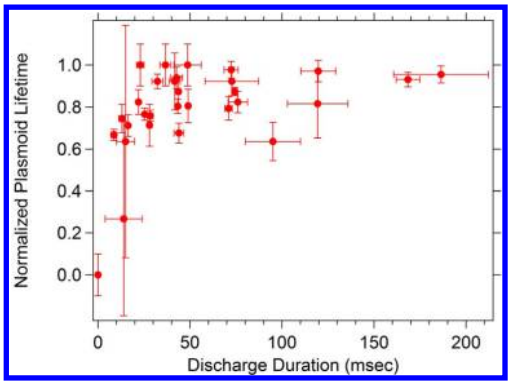

Figure 5. Comparison of the lifetime of the plasmoid with the duration of the discharge. Each of the data points has been normalized to the peak lifetime observed for a given voltage and capacitance. These results suggest that there is an optimal time window in which to discharge the current into the electrolyte and have it influence the lifetime of the plasma.

more closely by recording the plasmoid lifetime for many more resistivity values, a topic of future work.

The results in Figure 4 imply that the conditions for producing the longer-lived plasmoids have not yet been reached (high voltage and resistivity), although there is evidence that the lifetime is saturating based on the diminishing increases in lifetime with capacitance. Figure 6 displays the same data set

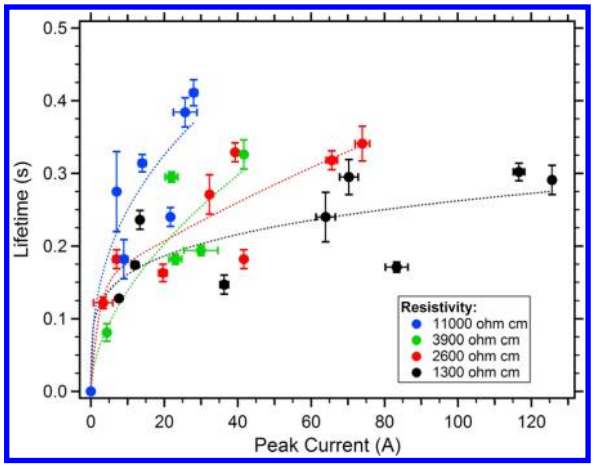

Figure 6. Lifetime of the plasmoids versus peak discharge current for different electrolyte resisitivities. These data have been fit to a power function to guide the eye. Saturation effects are clearly observable at higher peak currents, although its onset appears to be delayed with higher resistivities. The remaining scatter in the data is due to other effects (such as discharge duration and total energy) not being normalized out.

plotted instead versus the peak discharge current for different electrolyte resistivities, each fit to a power function (dashed lines) to help guide the eye. From these data it is clear that the higher discharge currents lead to longer plasmoid lifetimes and that there is a clear saturation effect. Interestingly, the onset of saturation effect is lessened at higher resistivities, an indication that longer lifetimes are still achievable. There is a need to examine yet higher resisitivites and voltages to test this hypothesis, measurements that lie outside the scope of this work.

It has been suggested by Shevkunov and others[43−45] that the stabilization of a plasmoid (and perhaps ball lightning) may be

dx.doi.org/10.1021/jp400001y | J. Phys. Chem. A XXXX, XXX, XXX−XXX

due to the highly hydrated ions/ionized water clusters/aerosols. If so, it may be reasonable to expect, then, that the plasmoid will be sensitive to the pH of the electrolyte in addition to its resistivity. To test this hypothesis, we measured the lifetime of the plasmoid as the pH of the electrolytic solution was varied from acidic (pH 3.7) to neutral (pH 5.7) to basic (pH 10.2) by utilizing HCl and NaOH. In each case, the resistivity of the electrolyte was maintained by varying amounts of NaCl. Figure 7 shows the results of these measurements for an 860 μF

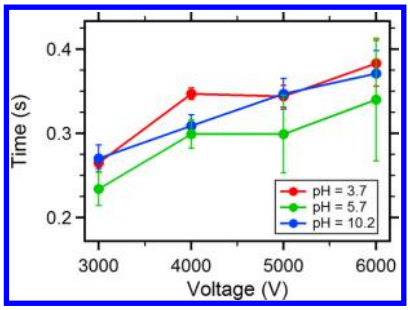

Figure 7. Lifetime of the plasmoids versus initial discharge voltage onto acidic (pH 3.7), neutral (pH 5.7), and basic (pH 10.2) electrolyte solutions. The resistivity of the electrolyte was kept fixed at 5.0 kΩ·cm by adding NaCl to the solution after the pH was adjusted with HCl and NaOH. The capacitance for each of these measurements was fixed at 860 μF, and the error bars represent one standard deviation of the measurements.

capacitor charged to different voltages and discharged into a solution with a resistivity of 5.0 kΩ·cm. Interestingly, there is a small but statistically significant effect of pH; the plasmoid's lifetime increases as the solution deviates from neutrality. The observed increase is only ∼10% of the lifetime, however, and appears to be equally effected by the presence of hydroxide and hydronium ions. The fact that only a small effect on the plasmoid lifetime is observed when the H_3O^+ and OH^- concentrations are varied by over six orders of magnitude is remarkable and suggests that ions already present in the electrolyte may not play a major role in the longevity of the plasmoid aside from affecting the discharge current.

Infrared Absorption Spectrum. To examine its molecular composition, we measured the infrared absorption spectrum of the plasmoid using a fiber-coupled FTIR. Figure 8 contains overlaid averaged transmission spectra of the two regions measured with different fiber optics. For each of these measurements, the infrared beam passed horizontally over the center of the electrolyte, located 15 cm above the cathode. While the signal-to-noise ratio of the spectrum is rather low due to the ephemeral nature of the plasmoid, several absorption features are conclusively observed.

The strongest feature is a sharp absorption located between 2280 and 2390 cm^{-1} and is characteristic of the asymmetric stretching mode of gaseous CO_2. Also associated with CO_2 is the weaker bending mode from 620 to 700 cm^{-1}, which is weakly observed in this spectrum. Interestingly, the intensity of these features was observed to fluctuate as much as 75% from event to event, whereas the other peaks were more constant. This behavior and the lack of carbon present in the electrolyte leads us to conclude that it is due to the oxidation of the graphite electrode, perhaps assisted by chemistry within the plasmoid.

The next strongest absorption has a complex structure and is observed between 3300 and 4000 cm^{-1}. Most of these

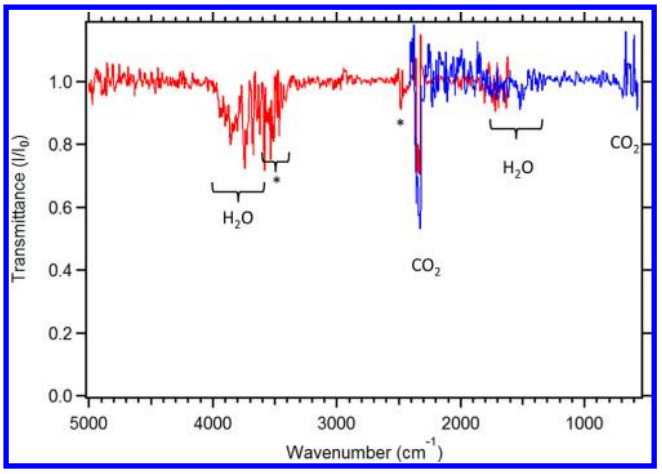

Figure 8. Infrared transmission spectra of plasmoids as obtained from a fiber-optic-coupled FTIR after removing the background atmospheric absorptions. The beam of the spectrometer crosses over the top of the electrolyte solution 15 cm above the cathode. In addition to the presence of gas-phase H_2O and CO_2, two unassigned features are observed and denoted with an asterisk. The spectrum from 1500 to 5000 cm^{-1} (red) was obtained using CIR fiber-optic cables, and the spectrum from 550 to 2300 cm^{-1} (blue) was obtained using PIR fiber-optic cables.

absorption features are easily attributed to the two OH stretching bands of gas-phase H_2O. Also expected from gas-phase H_2O is the bending band, located between 1500 and 1700 cm^{-1}, which appears to be present just above the noise floor. Interestingly, there is little evidence of the presence of water fog, which we would expect to see as a broad, low-resolution feature in this same region.[46] It is possible, however, that such a spectrum is being masked by the strong H_2O absorptions, and so its presence cannot be completely dismissed.

Two absorption features remain unassigned, denoted by asterisks in Figure 8. The first are features overlapping with the H_2O band and shifted to lower wavenumber. These features are well known to be the location of ionized and water clusters, including $H^+(H_2O)_n$ (n = 2,3), $OH^-(H_2O)_n$ (n = 5,6), and neutral water clusters.[47−50] Another unassigned absorption is observed at slightly higher wavenumber than the asymmetric stretch of CO_2 between 2400 and 2500 cm^{-1}. Whereas this is an uncommon region for vibrational absorptions, the asymmetric stretch of CO_2 is known to shift into this region when in the presence of water due to the formation of an electron donor−acceptor complex.[51] The likelihood that the plasmoid can support the formation of such water clusters/complexes is unknown. Given that the plasma's gas temperature is over 1300 K for the first 200 ms after a discharge,[36] it is thermodynamically unlikely that water could cluster around hydroxide and hydronium ions at early times.[52] However, water clustering may be occurring near the boundary of the plasma and at later times, and water molecules may still be able to inhibit recombination without clustering. This is clearly a topic that needs further investigation and suggests the importance of obtaining a higher resolution spectrum of these unassigned features so that their structures can be identified.

Unfortunately, a quantitative measure of the concentration of CO_2 and H_2O present was not possible with the available instrumentation. Given our inability to trigger the scanning of the spectrometer with the discharge, samples were taken across

dx.doi.org/10.1021/jp400001y | J. Phys. Chem. A XXXX, XXX, XXX−XXX

a three-second interval of the event that was only ~0.5 s in duration. Experiments using other techniques such as step-scan FTIR and transient absorption spectroscopies are being considered and are expected to provide higher spectral resolution, time response, sensitivity required to deduce the concentration, and carriers for the observed infrared absorption features.

Schlieren Imagery. A progression of images of the plasmoid obtained by the schlieren videography is presented in Figure 9. This specific trial shows the initial production of two separate balls by the discharge and shows that the smaller one ('B') is consumed into the larger one ('A') after ~250 ms. All of the plasmoids observed exhibited the features of a toroidal vortex, similar to a smoke ring or mushroom cloud. We also observe in this series of images that a small, fast moving spark and its heated track in air is present at the top of the image in the first few frames (dashed circled). Such sparks occur occasionally and are attributed to a small amount of material ablating from the cathode during the discharge.

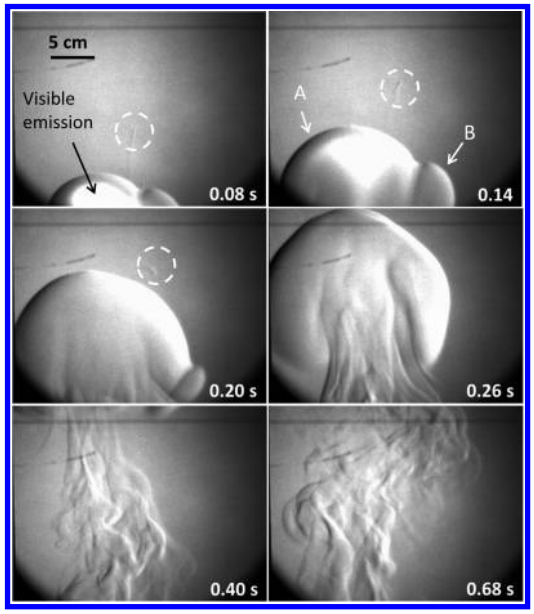

Figure 9. Progression of video images taken through schlieren optics of a plasmoid produced by discharging an 860 μF capacitor charged to 5 kV across a 7.7 kΩ·cm $CuSO_4$ solution. In addition to capturing the schlieren image, visible emission, similar to what was is presented in Figure 2, was also observed. Images were taken with a high-speed Phantom Camera and a vertically aligned knife edge. A 5 cm scale bar is added to the upper left frame to establish the scale, and the bottom of each frame is located ~3.5 cm above the top of the cathode. In this example, two plasmoids are initially formed, and the smaller (B) is absorbed into the larger (A) ~250 ms after initiation of the discharge. A spark (highlighted by the dashed circled), presumably ablating from the cathode, is observed to eject ahead of the plasmoid.

It is important to emphasize that the schlieren technique is sensitive to changes in index of refraction through a transparent media. The intensity variation observed in the images is therefore a measure of changes in material composition, density, and temperature. These images clearly show that the optical density of the plasmoid is substantially different from the density of the air, as is evidenced by the high-contrast intensity observed between the right and left side of the plasmoid (schlieren contrast). The images also reveal that the plasmoid has a smooth and homogeneous index of refraction within the ball aside a small amount of turbulent structure at the center. This smoothness is likely an indication that the composition, density, and temperature within the plasmoid are fairly homogeneous, although we cannot rule out that several properties of the plasmoid are varying in such a way that the index of refraction remains constant. The turbulent tail observed below the ball is probably not due to material remnants from the plasmoid but is attributed to mixing flow of the ambient air after the passing warm body as well as convection above the still-hot cathode.

Also picked up by the high-speed camera on the first three schlieren images is the bright visible emission (bright white light from the plasmoid). Interestingly, this emission appears to be emanating from within the center of plasmoid and set back from the sharp edge of the ball by ~1 cm. This set-back appears to be even larger than the boundary layer observed by others[35,39] and suggests that the data obtained from previous experiments, which were mostly emission based, captured only the inner core of the object. The previously reported Faraday probe measurement observed a skin of negative charge[28] that may be associated with regions of no optical emission. The center of the plasmoid, where the emission emerges, has been measured to have a positive charge attributed to metal ions.[35] The fact that the schlieren density measurements show no signs of a sharp boundary within the bulk of the plasmoid is an indication that the heterogeneous ion distributions do not lead to large heterogeneity in mass density or in translational temperature across the plasmoid. It is still possible, however, that the perceived temperature could be significantly varied across the plasmoid as a result of the differing chemistry.

Given the ease of 'seeing' the boundary of the plasmoid in the schlieren images, it was straightforward to track its location and diameter as a function of time. Figure 10 plots the diameter, center height, and the volume of the plasmoid depicted in Figure 9, as determined by the best fit circle to the plasmoid for each frame. The camera was stationary for each of these shots, and the height is relative to the top of the cathode. For frames where the plasmoid was not in complete view, we

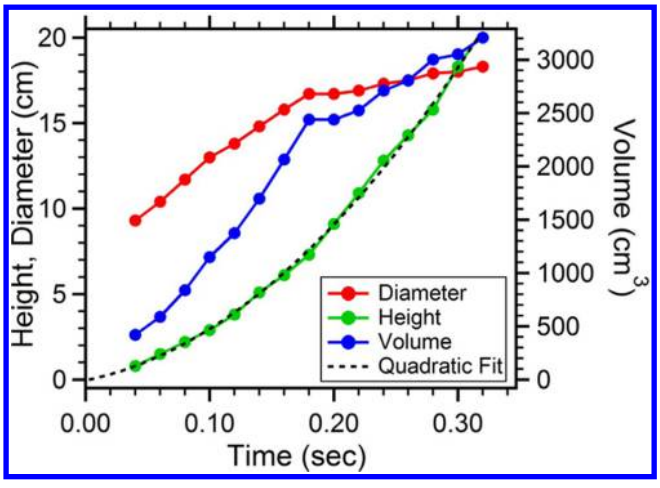

Figure 10. Diameter and height (left axis, red and green trace) of the plasmoid versus time as obtained from the schlieren video. Also plotted is the apparent volume of the plasmoid (right axis, blue trace) versus time based on the diameter of the ball versus time. The plasmoid is found to be vertically accelerating at a constant rate of 3.1 m/s^2, as determined by the quadratic fit of the height versus time (dashed line).

dx.doi.org/10.1021/jp400001y | J. Phys. Chem. A XXXX, XXX, XXX−XXX

assumed it maintained a spherical shape to estimate its height, diameter, and volume. These results indicate that the volume of the plasmoid increases approximately linearly in time and that the height of the center of the plasmoid is accelerating upward at a constant rate of 3.1 m/s^2 (quadratic fit, dashed line.) Assuming this acceleration is due solely to buoyancy, the average density of the plasma is found to be 66% that of air, using the buoyancy equation, $\rho_{plasma} = \rho_{atm} \times ((g - a/g + a))$, where ρ_{atm} and ρ_{plasma} are the densities of air and the plasmoid, g is 9.8 m/s^2, and a = 3.1 m/s^2 is the vertical acceleration of the plasmoid. This simplified relationship is based on a balance of forces and assumes that frictional forces are negligible and that the density of the plasmoid remains constant during the expansion. The former assumption is reasonable given that gases are involved and that the velocity is low. The latter assumption is based on the fact that we observe a constant acceleration on the plasmoid (i.e., height increases with a t^2 dependence, quadratic fit in Figure 10). Given that the plasmoid expands in volume by a factor of ∼10 over the course of the images, there must be an increase in mass within the plasmoid if the density remains constant. Over most of the time probed in these measurements the discharge continues to "feed" the plasmoid with additional warm mass and is responsible for some of the expansion. This is consistent with the observation that the rate of increase in diameter tapers off after 150 ms, which is coincident with the completion of the discharge pulse.

CONCLUSIONS

Applying new diagnostics has provided additional insights into the nature of the atmospheric pressure plasmoids. Examining the dependence of the discharge parameters on the plasmoid's behavior has confirmed previous reports that both higher voltages and capacitances increase the lifetime and size of the plasmoid for a given resistivity. Additionally, electrolyte solutions with higher resistivity were found to produce longer-lived plasmoids when discharges were driven by higher voltages. These observations are attributed to an optimum time frame in which to discharge the current into the electrolyte and have it be involved in the plasmoid formation process. Discharging too quickly produced ionized mass before the plasmoid has a chance to completely form, while discharging too slowly results in the plasmoid departing from the discharge region before additional mass can be added. Measurements of the plasmoid's lifetime for different pH electrolytes showed only a slight (∼10%) dependence on OH^- and H_3O^+ concentration. The small increase in lifetime for a six order of magnitude change in concentration suggests that the ions present in the electrolyte play little role in the formation of the plasma aside from establishing the resistivity of the discharge.

Infrared absorption measurements reveal the presence of gas phase water and carbon dioxide in the plasmoid, the latter likely produced from the combustion of graphite particles from the cathode. Two additional features are left unassigned, but show similarities to ionized and neutral clusters of water and neutral water−carbon dioxide complexes. Definitively assigning such features will require higher resolution and higher sensitivity spectra, and may hold the key to understanding the chemistry within the plasmoids.

Schlieren videography has revealed new information on the structure of the plasmoid. First, a sharp and distinct boundary layer is observed that is ∼1 cm larger than that of the luminous portion of the plasmoid. Second, the density distribution within the plasmoid appears to be fairly uniform, with the exception of some turbulent heterogeneity near its core, a structure consistent with a toroidal vortex. Below the plasmoid exists what appears to be turbulent mixing, presumably a consequence of the passing warm plasmoid through air and convective heating from the still warm cathode. The clear images of the plasmoid's size revealed that its volume increases linearly in time and that the body is accelerating upward. Assuming that this is due to buoyancy, we estimate the average density of the plasmoid to be 66% that of the surrounding atmosphere.

Given the shape of the ball observed in the schlieren images, the increased CO_2 absorbance apparent in the plasmoids in the infrared spectra, and the appearance of absorptions gaseous water as well as possible water−ion clusters, we conclude that the plasmoid is displacing air with a warm, partially ionized water−aerosol produced by the discharge. This is indeed consistent with the ball-lightning models proposed by Shevkunov,[43−45] where cation−anion recombination is inhibited by many orders of magnitude by the clustering of water around ion atomic and molecular ion cores. While these results will continue to shed light on the nature of these particular laboratory-produced plasmas, whether or not this phenomenon is responsible for the naturally occurring ball lightning remains an open question. Given the technical challenges and improbability that scientific instrumentation can be brought to bear on natural ball lightning, efforts would need to be made to lengthen the lifetime of these plasmoids to several seconds (the time scales of most reports in nature) and observe their long-lifetime behavior before such results can be convincing. Efforts are underway to explore higher voltage and resistivity regimes where the lifetimes are expected to be longer.

AUTHOR INFORMATION

Corresponding Author

*E-mail: c.lindsay@us.af.mil. Phone: (850) 882-1543. Fax: (850) 882-3540.

Present Address

†C. Michael Lindsay: AFRL/RWME Air Force Research Laboratory, Eglin AFB, Florida, 32542, United States.

Notes

The authors declare no competing financial interest.

ACKNOWLEDGMENTS

We gratefully acknowledge the assistance of Eric Stephen and Tim Hayden from the department of Aeronautic Engineering at the United States Air Force Academy in obtaining the schlieren images of the plasmoids. We also wish to thank Russ Maines and Mark Heyse at the Air Force Research Laboratory for donating and shipping the large capacitors used here. This research was initiated while C.M.L. served as a Visiting Professor of Chemistry at the United States Air Force Academy. This work was supported by the Small Grant Program from the Air Force Office of Scientific Research.

REFERENCES

(1) Oka, T. Spectroscopy and Astronomy: H_3^+ from the Laboratory to the Galactic Center. *Faraday Discuss.* **2011**, *150*, 9−22.

(2) Oka, T. The Infrared-Spectrum of H_3^+ in Laboratory and Space Plasmas. *Rev. Mod. Phys.* **1992**, *64*, 1141−1149.

(3) Oka, T. Extraordinary Molecules in Interstellar Space. In *Atomic Physics 10, Proceedings of the Tenth International Conference on Atomic*

Physics (ICAP-X) held in Tokyo, August 25−29, 1986; Narumi, H., Shimamura, I., Eds.; North-Holland: Amsterdam, 1987; p 439.
(4) Wakelam, V.; Smith, I. W. M.; Herbst, E.; Troe, J.; Geppert, W.; Linnartz, H.; Öberg, K.; Roueff, E.; Agúndez, M.; Pernot, P.; et al. Reaction Networks for Interstellar Chemical Modelling: Improvements and Challenges. *Space Sci. Rev.* **2010**, *156*, 13−72.
(5) Ter Haar, D. An Electrostatic-Chemical Model of Ball Lightning. *Phys. Scr.* **1989**, *39*, 735−740.
(6) Abrahamson, J. J. Ball Lightning from Atmospheric Discharges via Metal Nanosphere Oxidation: from Soils, Wood or Metals. *Philos. Trans. R. Soc., A* **2002**, *360*, 61−88.
(7) Donoso, J. M.; Trueba, J. L.; Rañada, A. F. The Riddle of Ball Lightning: A Review. *Sci. World J.* **2006**, *6*, 254−278.
(8) Meshcheryakov, O. Ball Lightning-Aerosol Electrochemical Power Source or a Cloud of Batteries. *Nanoscale Res. Lett.* **2007**, *2*, 319−330.
(9) Stephan, K. D. Electrostatic Charge Bounds for Ball Lightning Models. *Phys. Scr.* **2008**, *77*, 035504.
(10) Shavlov, A. V. The Two-Temperature Plasma Model of a Fireball: The Calculated Parameters. *Phys. Lett. A.* **2009**, *373*, 3959−3964.
(11) Meshcheryakov, O. Charge-Dipole Acceleration of Polar Gas Molecules towards Charged Nanoparticles: Involvement in Powerful Charge-Induced Catalysis of Heterophase Chemical Reactions and Ball Lightning Phenomenon. *J. Nanomater.* **2010**, *2010*, 654389.
(12) Tennakone, K. Stable Spherically Symmetric Static Charge Separated configuration in the Atmosphere: Implications on Ball Lightning and Earthquake Lights. *J. Electrost.* **2011**, *69*, 638−640.
(13) McNally, J. R. *Preliminary Report on Ball Lightning*, No. 3938.; Oak Ridge National Laboratory: Oak Ridge, TN, 1966,
(14) Charman, W. N. Ball Lightning. *Phys. Rep.* **1979**, *54*, 261−306.
(15) Smirnov, B. M. Physics of Ball-Lightning. *Phys. Rep.* **1993**, *224*, 151−236.
(16) Tesla, N. *Colorado Springs Notes 1899−1900*; Marinčić, A., Ed.; Nolit: Beograd, Yugoslavia, 1978; pp 368−370.
(17) Singer, S. *The Nature of Ball Lightning*; Plenum: New York, 1971; p 63.
(18) Barry, J. D. *Ball Lightning and Bead Lightning*; Plenum: New York, 1980; pp 25−27, 59−60, 180−182.
(19) Kapitza, P. L. Über die Natur des Kugelblitzes. *Phys. Blätter* **1958**, *14*, 11.
(20) Kapitza, P. L. Ball Lightning and Radio Emission from Linear Lightning. *Sov. Phys. Tech. Phys.(Engl. Transl.)* **1969**, *13*, 1475.
(21) Golka, R. K. Laboratory-Produced Ball Lightning. *J. Geophys. Res.* **1994**, *99* (D5), 10679−10681.
(22) Hill, J. D.; Umann, M. A.; Stapleton, M.; Jordan, D. M.; Chebaro, A. M.; Biagi, C. J. Attempts to Create Ball Lightning with Triggered Lightning. *J. Atmos. Sol.-Terr. Phys.* **2010**, *72*, 913−925.
(23) Abrahamson, J.; Dinnis, J. Ball Lightning Caused by Oxidation of Nanoparticle Networks from Normal Lightning Strikes on Soil. *Nature* **2000**, *403*, 519−521.
(24) Lazarouk, S. K.; Dolbik, A. V.; Labunov, V. A.; Borisenko, V. E. Spherical Plasmoids Formed upon the Combustion and Explosion of Nanostructured Hydrated Silicon. *JETP Lett.* **2006**, *84*, 581−584.
(25) Paiva, G. S.; Pavão, A. C.; Alpes De Vasconcelos, E.; Mendes, O.; Felisberto Da Silva, , E. Production of Ball-Lightning-Like Luminous Balls by Electrical Discharges in Silicon. *Phys. Rev. Lett.* **2007**, *98*, 048501.
(26) Egorov, A. I.; Stepanov, S. I. Long-Lived Plasmoids Produced in Humid Air as Analogues of Ball Lightning. *Tech. Phys.* **2002**, *47*, 1584−1586.
(27) Egorov, A. I.; Stepanov, S. I.; Shabanov, G. D. Laboratory Demonstration of Ball Lightning. *Phys.-Uspekhi.* **2004**, *47*, 99−101.
(28) Egorov, A. I.; Stepanov, S. I. Properties of Short-Living Ball Lightning Produced in the Laboratory. *Tech. Phys.* **2008**, *53*, 688−692.
(29) Sakawa, Y.; Sugiyama, K.; Tanabe, T.; More, R. Fireball Generation in a Water Discharge. *Plasma Fusion Res. Rapid Commun.* **2006**, *1*, 039.
(30) Hayashi, N.; Satomi, H.; Kajiwara, T.; Tanabe, T. Properties of Ball Lightning Generated by a Pulsed Discharge on Surface of an Electrolyte in the Atmosphere. *IEEJ Trans. Electr. Electron. Eng.* **2008**, *3*, 731−733.
(31) Hayashi, N.; Satomi, H.; Kajiwara, T.; Tanabe, T. General Nature of Luminous Body Transition Produced by Pulsed Discharge on an Electrolyte Solution in the Atmosphere. *IEEJ Trans. Electr. Electron. Eng.* **2009**, *4*, 674−676.
(32) Bulgakov, A. A.; Yefimov, B. P.; Kuleshov, A. N.; Khorunzhiy, M. O. Experimental Investigation into Spherical Plasma Formations. *Telecommun. Radio Eng. (Engl. Transl.)* **2005**, *64*, 833−839.
(33) Bulgakov, A. A.; Yefimov, B. P.; Khutoryan, E.; Khorunzhiy, M.; Kuleshov, A. Excitation and Observation of Ball-Lightning Type Spherical Formations. In *Conference Proceedings: the 12th International Conference on Mathematical Methods in Electromagnetic Theory: MMET *08: Odesa, Ukraine, June 29−July 02, 2008*; IEEE: Piscataway, NJ, 2008.
(34) Khorunzhiy, M. O.; Kuleshov, A. N.; Yefimov, B. P. Long-Living Plasma Excited by Electric Discharge in Water. *IEEE Trans. Plasma Sci.* **2011**, *39*, 2648−2649.
(35) Juettner, B.; Noack, S.; Versteegh, A.; Fussmann, G. Long-Living Plasmoids from a Water Discharge at Atmospheric Pressure. In *XXVIII International Conference on Phenomena in Ionized Gases: July 15-20, 2007, Prague, Czech Republic: Book of Abstracts: ICPIG 2007*; Institute of Plasma Physics: Prague, 2007; pp 2229−2234
(36) Versteegh, A.; Berhringer, K.; Fantz, U.; Fussmann, G.; Jüttner, B.; Noack, S. Long-Living Plasmoids from an Atmospheric Water Discharge. *Plasma Sources Sci. Technol.* **2008**, *17*, 024014.
(37) Noack, S.; Versteegh, A.; Jüttner, B.; Fussmann, G. Analysis of Long-Living Plasmoids at Atmospheric Pressure. *AIP Conf. Proc.* **2008**, *933*, 129−132.
(38) Fantz, U.; Briefi, S.; Friedl, R.; Kammerloher, M.; Oswald, A.; Rauner, D. Relaunch of the Water Plasmoid Experiment for Investigations of Ball Lightning Phenomena. In *Proc. of the 30th ICPIG*; Queen's University: Belfast, U.K., 2011, *C10−329* pp 1−4.
(39) Wurden, C. J.; Wurden, G. A. Free-Floating Atmospheric Pressure Ball Plasmas. *IEEE Trans. Plasma Sci.* **2011**, *39*, 2078−2079.
(40) Morgan, W. L.; Rosocha, L. A. Surface Electrical Discharges and Plasma Formation on Electrolyte Solutions. *Chem. Phys.* **2012**, *398*, 255−261.
(41) Wurden, G. A. Personal Communication, Los Alamos National Laboratory, Los Alamos, NM, 2010.
(42) Settles, G. S. *Schlieren and Shadowgraph Techniques: Visualizing Phenomena in Transparent Media*, 1st ed.; Springer-Verlag: New York, 2001.
(43) Shevkunov, S. V. Scattering of Centimeter Radiowaves in a Gas Ionized by Radioactive Radiation: Cluster Plasma formation. *J. Exp. Theor. Phys.* **2001**, *92*, 420.
(44) Shevkunov, S. V. Cluster Mechanism of the Energy Accumulation in a Ball Electric Discharge. *Dokl. Phys.* **2001**, *46*, 467.
(45) Shevkunov, S. V. A High Energy Barrier to Charge Recombination in Ionized Water Vapor. *High Energy Chem.* **2009**, *43*, 341−349.
(46) Kalashnikova, O. V.; Willebrand, H. A.; Mayhew, L. M. Wavelength and Altitude Dependence of Laser Beam Propagation in Dense Fog. *Proc. SPIE* **2002**, *4635*, 278−287.
(47) Headrick, J. M.; Diken, E. G.; Walters, R. S.; Hammer, N. I.; Christie, R. A.; Cui, J.; Myshakin, E. M.; Duncan, M. A.; Johnson, M. A.; Jordan, K. D. Spectral Signatures of Hydrated Proton Vibrations in Water Clusters. *Science* **2005**, *308*, 1765−1769.
(48) Jieli, M.; Aida, M. Classification of OH Bonds and Infrared Spectra of the Topology-Distinct Protonated Water Clusters $H_3O^+(H_2O)_{n-1}$($n \leq 7$). *J. Phys. Chem. A* **2009**, *113*, 1586−1594.
(49) Reimer, J. R.; Watts, R. O. The Structure and Vibrational Spectra of Small Clusters of Water Molecules. *Chem. Phys.* **1984**, *85*, 83−112.
(50) Robertson, W. H.; Diken, E. G.; Price, E. A.; Shin, J.; Johnson, M. A. Spectroscopic Determination of the OH^- Solvation Shell in the $OH^-{\cdot}(H_2O)_n$ Clusters. *Science* **2003**, *299*, 1367−1372.

(51) Danten, Y.; Tassaing, T.; Besnard, M. Ab Initio Investigation of Vibrational Spectra of Water-$(CO_2)_n$ complexes (n=1, 2). *J. Phys. Chem. A* **2005**, *109*, 3250−3256.
(52) Shevkunov, S. V. Structural Transition in the $OH^-(H_2O)_n$ Cluster in Water Vapors. *Colloid J.* **2008**, *70*, 784−795.